Institute of
Applied Mechanics
Institut für Baumechanik

Graz University of Technology

Preprint Series

Institute of Applied Mechanics

Graz University of Technology

Preprint No 4/2008

An alternative collocation boundary element method for static and dynamic problems

Thomas Rüberg
Institute for Structural Analysis, Graz University of Technology

Martin Schanz
Institute of Applied Mechanics, Graz University of Technology

Published in: *Computational Mechanics*, volume 44,
pages 247–261, 2009

Latest revision: January 16, 2009

Abstract

A collocation boundary element formulation is presented which is based on a mixed approximation formulation similar to the Galerkin boundary element method presented by Steinbach [39] for the solution of Laplace's equation. The method is also applicable to vector problems such as elasticity. Moreover, dynamic problems of acoustics and elastodynamics are included. The resulting system matrices have an ordered structure and small condition numbers in comparison to the standard collocation approach. Moreover, the employment of Robin boundary conditions is easily included in this formulation. Details on the numerical integration of the occurring regular and singular integrals and on the solution of the arising systems of equations are given. Numerical experiments have been carried out for different reference problems. In these experiments, the presented approach is compared to the common nodal collocation method with respect to accuracy, condition numbers, and stability in the dynamic case.

The original publication will be available at www.springerlink.com with the Digital Object Identifier (DOI): 10.1007/s00466-009-0369-4

1 Introduction

The most prominent boundary element method in structural engineering remains the nodal collocation method in which the approximated boundary integral equation is evaluated on the interpolation nodes. This method has been applied to numerous static and dynamic engineering problems [5, 6, 10]. Nodal collocation methods yield system matrices of rather small size which are dense, nonsymmetric and often ill-conditioned. In these methods, the dual variable (e.g., surface fluxes or tractions) are commonly approximated with the same continuous polynomials as the primal variable (e.g., potentials or displacements). But these data have different mathematical and physical properties [41]. In fact, the dual variable is not uniquely defined at corners and edges of the considered geometry [26] and is thus discontinuous. See also [43] for a consideration of the so-called *corner problem*. A common approach to handle these natural discontinuities is the introduction of additional data points at corners and edges [26]. Although feasible, this approach requires that either the user places these additional nodes or that the computer code is capable to do this job automatically. Both situations are unsatisfactory and yield a significant amount of additional work.

There are many early works on the use of discontinuous elements for circumventing the problems arising from the discontinuous nature of the dual variable. For instance, the publications of Patterson and co-authors [27–29] propose the use of discontinuous elements for various problems in two and three spatial dimensions. See also the discussion in [26]. Partially discontinuous elements are also proposed in [29] but no algorithm is given which can detect the locations automatically where these functions shall be used and where not. Finally, it has to be stated that in all these approaches both the primal and the dual variable are approximated with the same type of functions. Therefore, either both are discontinuous, partially discontinuous, or continuous. But this concept ignores the fact the primal variable is a (mathematically and physically) continuous function and, therefore, it seems more sound to treat these fields independently.

Alternatively, the symmetric Galerkin boundary element [41] method has come up which is based on a weighted residual concept and makes use of two boundary integral equations. The primal and dual variables are approximated independently in the correct mathematical subspaces and the corner problem does therefore not exist anymore. These Galerkin schemes yield symmetric positive definite system matrices and show a robust performance. Nevertheless, the second integral equation is hypersingular and, therefore, needs sophisticated regularization techniques. One approach to treat hypersingular integrals is based on integration by parts. For the case of the Laplace's equation and the elastostatic system, such a regularization is given in [41]. The regularization of hypersingular kernels for the elastodynamic system (as presented below) is given in [16]. Moreover, the computational cost to generate a single matrix entry is significantly higher than in the collocation method.

In this work, an alternative collocation approach is presented which uses different approximations for primal and dual boundary unknowns. Whereas the former is still approximated by continuous functions, the latter is taken to be discontinuous across the element edges. Therefore, unique solutions of the dual variable are facilitated. The collocation points are placed strictly inside the elements such that the expressions for the integral-free term become trivial. The prescribed Dirichlet boundary condition will be fulfilled directly by the approximation and the Neumann boundary condition is employed by means of a side condition weighted by the

shape functions of the primal approximation. With this technique a structured system of equations is obtained which shows a good conditioning in comparison with the standard collocation approach. A Galerkin variant of the presented collocation approach has been introduced and mathematically analyzed in [39]. In this reference, the method is presented for a general elliptic partial differential operator and the numerical results refer to Laplace's equation. Note that the stability issues in [39] also appear here and this problem is addressed at the end of section 5. Moreover, Robin boundary conditions are easily included in this approach and do not require column manipulations of the system matrix or additional side conditions.

The outline of the paper is to present at first the basic equations in operator notation in section 2. By means of this abstraction, it is easier to consider scalar and vector problems with the same notation. The equations are given for static and dynamic problems. Then the spatial and temporal discretizations are presented in section 3, where the convolution quadrature method is used for the dynamic problems. Afterwards in section 4, the used numerical integration is explained for the regular and singular surface integrals. A quick description of the used direct solution routine follows in section 5. Various numerical examples are given with a direct comparison to nodal collocation results and analytical reference solutions in section 6. Finally section 7 contains a discussion of the advantages and disadvantages of the presented method and it closes the paper. At all crucial points, the differences to the nodal collocation approach are emphasized.

2 Basic equations

2.1 Boundary value problems

The considered mathematical models in this work are mixed elliptic boundary value problems and hyperbolic initial boundary value problems. On the one hand, Laplace's equation and the elastostatic system are the elliptic (or static) representatives, see [41], and, on the other hand, the scalar wave equation and the elastodynamic system are the chosen examples of hyperbolic (or dynamic) Eqs. [1]. For sake of legibility, let $\mathcal{L}$ denote an elliptic partial differential operator with constant coefficients and u is a generic unknown representing, for instance, the acoustic pressure or the displacement field of an elastic solid. For the models of this work, it holds either $\mathcal{L}u = -\kappa\Delta u$, where κ is the conductivity or compressibility of the material and Δ denotes the Laplace operator, or $\mathcal{L}u = -(\lambda+2\mu)\nabla\cdot\nabla u + \mu\nabla\times\nabla\times u$, which is the Lamé-Navier [21] operator of elastostatics and λ and μ are the Lamé constants. Denoting the material density by ρ, the considered hyperbolic operators then become

$$(\mathcal{H}u)(\mathbf{x},t) = \rho\,\frac{\partial^2 u}{\partial t^2}(\mathbf{x},t) + (\mathcal{L}u)(\mathbf{x},t)\,. \tag{1}$$

By means of the above introduced notation, the considered mixed elliptic boundary value problem is of the form

$$\begin{aligned} (\mathcal{L}u)(\mathbf{x}) &= 0 && \mathbf{x}\in\Omega \\ u_\Gamma(\mathbf{y}) &= g_D(\mathbf{y}) && \mathbf{y}\in\Gamma_D \\ q(\mathbf{y}) = (\mathcal{T}u)(\mathbf{y}) &= g_N(\mathbf{y}) && \mathbf{y}\in\Gamma_N \\ q(\mathbf{y}) + \gamma(\mathbf{y})u_\Gamma(\mathbf{y}) &= 0 && \mathbf{y}\in\Gamma_R\,. \end{aligned} \tag{2}$$

This problem is stated for the d-dimensional domain Ω ($d = 2$ or $d = 3$) with boundary Γ which is composed of the Dirichlet, Neumann, and Robin boundaries, Γ_D, Γ_N, and Γ_R, respectively. The boundary trace of u is denoted by u_Γ, for which the datum g_D is prescribed on the Dirichlet boundary Γ_D. The operator $\mathcal{T}$ denotes the *traction* operator or co-normal derivative and maps the unknown u onto the surface flux or tractions q which are prescribed by g_N on the Neumann boundary. Robin boundary conditions combine the boundary data u_Γ and q by means of the positive function $\gamma(\mathbf{y})$ on the Robin boundary Γ_R. For simplicity, body forces or source terms are neglected.

In the dynamic case, the mixed initial boundary value problem looks like

$$\begin{aligned} (\mathcal{H}u)(\mathbf{x},t) &= 0 && (\mathbf{x},t) \in \Omega \times I_t \\ u_\Gamma(\mathbf{y},t) &= g_D(\mathbf{y},t) && (\mathbf{y},t) \in \Gamma_D \times I_t \\ q(\mathbf{y},t) &= g_N(\mathbf{y},t) && (\mathbf{y},t) \in \Gamma_N \times I_t \\ q(\mathbf{y},t) + \gamma(\mathbf{y}) u_\Gamma(\mathbf{y},t) &= 0 && (\mathbf{y},t) \in \Gamma_R \times I_t \,, \end{aligned} \tag{3}$$

where I_t is the considered time interval, e.g., $I_t = (0,T)$ with some positive time instant T. In addition to Eq. (3), initial conditions have to be prescribed for the starting time point. Here, a quiescent past [1] of the material is assumed and, therefore, the initial conditions are identical zero. Hence,

$$u(\mathbf{x},0^+) = 0 \quad \text{and} \quad \frac{\partial u}{\partial t}(\mathbf{x},0^+) = 0\,, \quad \mathbf{x} \in \Omega\,, \tag{4}$$

holds, where 0^+ denotes the limit $t \to 0$ from above. Note that for simplicity, the function γ in the Robin boundary conditions is assumed to be independent of time in the initial boundary value problem (3).

2.2 Boundary integral equations

It is well-known that the solution u of the mixed boundary value problem (2) at any point $\tilde{\mathbf{x}}$ *inside* the domain Ω is given by the representation formula [41]

$$u(\tilde{\mathbf{x}}) = \int_\Gamma U(\tilde{\mathbf{x}} - \mathbf{y}) q(\mathbf{y}) \, \mathrm{d}s_\mathbf{y} - \int_\Gamma (\mathcal{T}_\mathbf{y} U)(\tilde{\mathbf{x}} - \mathbf{y}) u_\Gamma(\mathbf{y}) \, \mathrm{d}s_\mathbf{y} \tag{5}$$

once the boundary data $[u_\Gamma, q]$ are known for the whole boundary Γ. In this expression, U denotes the full-space fundamental solution of the operator $\mathcal{L}$ and $\mathcal{T}_\mathbf{y} U$ is commonly referred to as flux or traction kernel. Note that the derivatives involved in the application of $\mathcal{T}_\mathbf{y}$ are with respect to the coordinate $\mathbf{y}$ as indicated by the subscript. Here, the fundamental solutions for elastostatics, the so-called Kelvin tensor [18, 21], and for Laplace's equation [10, 41] are employed.

The boundary trace $\Omega \ni \tilde{\mathbf{x}} \to \mathbf{x} \in \Gamma$ of Eq. (5) yields the first boundary integral equation which reads in operator form

$$(\mathcal{C} u_\Gamma)(\mathbf{x}) + (\mathcal{K} u_\Gamma)(\mathbf{x}) = (\mathcal{V} q)(\mathbf{x})\,. \tag{6}$$

$\mathcal{C}$ is the integral-free term and $\mathcal{V}$ and $\mathcal{K}$ are the single and double layer operators, respectively,

which are defined as [41]

$$\begin{aligned}(\mathcal{V}q)(\mathbf{x}) &= \int_\Gamma U(\mathbf{x}-\mathbf{y})q(\mathbf{y})\,\mathrm{d}s_\mathbf{y}\\ (\mathcal{K}u_\Gamma)(\mathbf{x}) &= \lim_{\varepsilon\to 0}\int_{\Gamma\setminus B_\varepsilon(\mathbf{x})} (\mathcal{T}_\mathbf{y}U)(\mathbf{x}-\mathbf{y})u_\Gamma(\mathbf{y})\,\mathrm{d}s_\mathbf{y}\\ (\mathcal{C}u_\Gamma)(\mathbf{x}) &= u_\Gamma + \lim_{\varepsilon\to 0}\int_{\partial B_\varepsilon(\mathbf{x})\cap\Omega} (\mathcal{T}_\mathbf{y}U)(\mathbf{x}-\mathbf{y})u_\Gamma(\mathbf{x})\,\mathrm{d}s_\mathbf{y}\,.\end{aligned} \tag{7}$$

In these definitions, $B_\varepsilon(\mathbf{x})$ is a ball of radius ε centered at $\mathbf{x}$ and $\partial B_\varepsilon(\mathbf{x})$ is its surface.

The mixed boundary value problem (2) can thus be solved by appropriate use of Eq. (6). A continuous extension $\tilde{g}_D$ of the given Dirichlet datum is introduced such that

$$\tilde{g}_D(\mathbf{x}) = g_D(\mathbf{x}) \quad \mathbf{x}\in\Gamma_D \tag{8}$$

holds. Moreover, the unknown boundary function u_Γ is now replaced by a new unknown

$$\tilde{u}_\Gamma = u_\Gamma - \tilde{g}_D\,, \tag{9}$$

which is defined on the whole boundary Γ. By means of the extension (8) and the new unknown (9), the boundary integral Eq. (6) becomes

$$(\mathcal{V}q)(\mathbf{x}) - (\mathcal{C}\tilde{u}_\Gamma)(\mathbf{x}) - (\mathcal{K}\tilde{u}_\Gamma)(\mathbf{x}) = (\mathcal{C}\tilde{g}_D)(\mathbf{x}) + (\mathcal{K}\tilde{g}_D)(\mathbf{x}) \tag{10}$$

for all $\mathbf{x}\in\Gamma$. For simplicity, the abbreviations

$$\tilde{\mathcal{K}} = (\mathcal{C}+\mathcal{K}) \quad \text{and} \quad f_D = \tilde{\mathcal{K}}\tilde{g}_D \tag{11}$$

are introduced, such that Eq. (10) finally reads

$$(\mathcal{V}q)(\mathbf{x}) - (\tilde{\mathcal{K}}\tilde{u}_\Gamma)(\mathbf{x}) = f_D(\mathbf{x})\,. \tag{12}$$

In addition, the Neumann and Robin boundary conditions have to be employed which require $q = g_N$ on Γ_N and $q+\gamma\tilde{u}_\Gamma = 0$ on Γ_R. Adding these conditions to the boundary integral Eq. (12), gives the system of operator equations

$$\begin{pmatrix}\mathcal{V} & -\tilde{\mathcal{K}}\\ \mathcal{I} & \mathcal{G}\end{pmatrix}\begin{pmatrix}q\\ \tilde{u}_\Gamma\end{pmatrix} = \begin{pmatrix}f_D\\ g_N\end{pmatrix} \tag{13}$$

with the identity operator $\mathcal{I}$ and the scaling operator $\mathcal{G}$, which basically multiplies the function γ with the unknown $\tilde{u}_\Gamma$.

In the hyperbolic case, the starting point is now the dynamic representation formula [1],

$$\begin{aligned}u_\Gamma(\mathbf{x},t) = &\int_0^t\int_\Gamma U(\mathbf{x}-\mathbf{y},t-\tau)q(\mathbf{y},\tau)\,\mathrm{d}s_\mathbf{y}\,\mathrm{d}\tau\\ &-\int_0^t\int_\Gamma (\mathcal{T}_\mathbf{y}U)(\mathbf{x}-\mathbf{y},t-\tau)u_\Gamma(\mathbf{y},\tau)\,\mathrm{d}s_\mathbf{y}\,\mathrm{d}\tau\,,\end{aligned} \tag{14}$$

where U is now the fundamental solution of the hyperbolic operator $\mathcal{H}$ as defined in Eq. (1). Again, the boundary trace yields the first dynamic boundary integral equation

$$(\mathcal{C}_t * u_\Gamma)(\mathbf{x},t) + (\mathcal{K}_t * u)(\mathbf{x},t) = (\mathcal{V}_t * q)(\mathbf{x},t)\,. \tag{15}$$

In this expression, $f * g$ denotes the temporal convolution, i.e., $f * g = \int_0^t f(t-\tau)g(\tau)\,\mathrm{d}\tau$ [42]. The occurring operators are now defined as

$$\begin{aligned}
(\mathcal{V}_t * q)(\mathbf{x},t) &= \int_0^t \int_\Gamma U(\mathbf{x}-\mathbf{y},t-\tau)q(\mathbf{y},\tau)\,\mathrm{d}s_\mathbf{y}\,\mathrm{d}\tau \\
(\mathcal{K}_t * u_\Gamma)(\mathbf{x},t) &= \\
&\lim_{\varepsilon\to 0} \int_{\Gamma\setminus B_\varepsilon(\mathbf{x})} \int_0^t (\mathcal{T}_\mathbf{y} U)(\mathbf{x}-\mathbf{y},t-\tau)u_\Gamma(\mathbf{y},\tau)\,\mathrm{d}s_\mathbf{y}\,\mathrm{d}\tau \\
(\mathcal{C}_t * u_\Gamma)(\mathbf{x},t) &= (\mathcal{C}\mathcal{I}_t * u_\Gamma)(\mathbf{x},t) = (\mathcal{C}u_\Gamma)(\mathbf{x},t)
\end{aligned} \tag{16}$$

with the same notation as in Eq. (7). In the expression of the integral-free term, the operator $\mathcal{I}_t = \mathcal{I}\delta(t)$ has been used for simplicity, which is the identity for the convolution, i.e., $\mathcal{I}_t * f = f$. Using again an extension of the prescribed Dirichlet datum g_D and an auxiliary unknown $\tilde{u}_\Gamma$, one arrives at the equation

$$(\mathcal{V}_t * q)(\mathbf{x},t) - (\tilde{\mathcal{K}}_t * \tilde{u}_\Gamma)(\mathbf{x},t) = f_D(\mathbf{x},t)\,, \tag{17}$$

where abbreviations analogously to Eq. (11) have been made, i.e., $\tilde{\mathcal{K}}_t = (\mathcal{C}_t + \mathcal{K}_t)$ and $f_D(\mathbf{x},t) = (\tilde{\mathcal{K}}_t * \tilde{g}_D)(\mathbf{x},t)$. The Neumann boundary conditions are again added as a side condition which is facilitated by the identity operator

$$(\mathcal{I}_t * q)(\mathbf{x},t) = g_N(\mathbf{x},t) \tag{18}$$

and, similarly, the Robin boundary condition is added by means of the expression

$$(\mathcal{I}_t * q)(\mathbf{x},t) + (\mathcal{G}_t * u_\Gamma)(\mathbf{x},t) = 0\,. \tag{19}$$

Here, the operator $\mathcal{G}_t = \mathcal{G}\delta(t)$ is defined in the same way as the identity $\mathcal{I}_t$ which is valid since the function γ has been assumed to be independent of time in the initial boundary value problem (3). The final system of operator equations then reads

$$\begin{pmatrix} \mathcal{V}_t & -\tilde{\mathcal{K}}_t \\ \mathcal{I}_t & \mathcal{G}_t \end{pmatrix} * \begin{pmatrix} q \\ \tilde{u}_\Gamma \end{pmatrix} = \begin{pmatrix} f_D \\ g_N \end{pmatrix}. \tag{20}$$

Classical approach. If the given Neumann datum g_N is extended in the same way, i.e., $\tilde{g}_N(\mathbf{x}) = g_N(\mathbf{x})$ on Γ_N, and a new boundary unknown $\tilde{q}$ is introduced by setting $\tilde{q} = q - \tilde{g}_N$, then Eq. (12) becomes

$$(\mathcal{V}\tilde{q})(\mathbf{x}) - (\tilde{\mathcal{K}}\tilde{u}_\Gamma)(\mathbf{x}) = f_D(\mathbf{x}) - (\mathcal{V}\tilde{g}_N)(\mathbf{x})\,. \tag{21}$$

Comparing Eqs. (12) and (21), it becomes clear that the way, the boundary unknown q is handled, is different. Whereas in Eq. (13) the Neumann boundary condition is used as a side condition and, therefore, the whole datum q is treated as an unknown function, in the classical approach (21) the known and unknown data are well separated. The main differences become clear when the discretizations are introduced. These observations can be directly transferred to the dynamic case.

3 Discretization

3.1 Spatial discretization

In the sense of a classical finite element discretization, the boundary Γ is now represented by the computational surface Γ_h which is the union of simple geometric entities, e.g., surface triangles or line elements in three or two spatial dimensions, respectively. With respect to this surface discretization, shape functions are defined for the spatial approximation of the unknown functions u_Γ and q, i.e.,

$$u_{\Gamma,h}(\mathbf{x}) = \sum_{i=1}^{N} \varphi_i(\mathbf{x}) u_i \quad \text{and} \quad q_h(\mathbf{x}) = \sum_{j=1}^{M} \psi_j(\mathbf{x}) q_j \,. \tag{22}$$

Note that this approximation has to be altered appropriately if u_Γ and q are vector fields, because then Eq. (22) has to be understood component-wise. Here, the functions φ_i are continuous functions as, for instance, the piecewise linear hat functions. The corresponding coefficients u_i are then the nodal unknowns of the approximation. On the contrary, the shape functions ψ_j are discontinuous and associated with the elements. Therefore, the coefficients q_j refer only to one specific element and the result can have jumps across the element boundaries. This choice of shape functions is fairly natural because, in case of elasticity problems, u_Γ represents the displacement field of the boundary which has to be continuous according to the assumptions of a continuum. On the other hand, the surface tractions q will have jumps at geometry corners and edges and, in addition, the corresponding Neumann datum g_N is often applied in form of a discontinuous function. Note that this choice is also consistent with the respective trace spaces [39, 41] corresponding to the data u_Γ and q in the boundary value problem (2).

The approximations (22) are also used for the given boundary data, $\tilde{g}_D$ and g_N, and for the auxiliary unknown $\tilde{u}_\Gamma$

$$\begin{aligned} \tilde{g}_{D,h}(\mathbf{x}) &= \sum_{i=1}^{N} \varphi_i(\mathbf{x}) \tilde{g}_{D,i} \\ g_{N,h}(\mathbf{x}) &= \sum_{j=1}^{M} \psi_j(\mathbf{x}) g_{N,j} \\ \tilde{u}_{\Gamma,h}(\mathbf{x}) &= \sum_{i=1}^{N} \varphi_i(\mathbf{x}) \tilde{u}_i \,. \end{aligned} \tag{23}$$

Inserting the approximations q_h, $u_{\Gamma,h}$, and $\tilde{g}_{D,h}$ into Eq. (12) yields a residual. In the sense of collocation techniques, this residual is then forced to be zero on a certain set of nodes $\{\mathbf{x}_\ell^*\}_{\ell=1}^{L} \subset$

Γ_h, the collocation points. This gives the discretized and collocated integral equation

$$\mathsf{V}\mathsf{q} - \mathsf{K}\mathsf{u} = \mathsf{f}_D\,. \tag{24}$$

These matrices have the following entries

$$\begin{aligned} \mathsf{V}[\ell,j] &= (\mathcal{V}\psi_j)(\mathbf{x}^*_\ell) \qquad \mathsf{q}[j] = q_j \\ \mathsf{K}[\ell,i] &= (\tilde{\mathcal{K}}\varphi_i)(\mathbf{x}^*_\ell) \qquad \mathsf{u}[i] = \tilde{u}_i \\ \mathsf{f}_D[\ell] &= (\tilde{\mathcal{K}}\tilde{g}_{D,h})(\mathbf{x}^*_\ell)\,. \end{aligned} \tag{25}$$

For completeness, the identities $q = g_N$ on Γ_N and $q + \gamma u_\Gamma = 0$ on Γ_R have to be added which is done in a weighted sense. This results in the matrix equation

$$\mathsf{B}\mathsf{q} + \mathsf{G}\mathsf{u} = \mathsf{f}_N \tag{26}$$

with the matrix coefficients

$$\begin{aligned} \mathsf{B}[k,j] &= \langle \varphi_k, \psi_j \rangle \qquad \mathsf{f}_N[k] = \langle \varphi_k, g_{N,h} \rangle \\ \mathsf{G}[k,i] &= \langle \varphi_k, \gamma\varphi_i \rangle\,. \end{aligned} \tag{27}$$

Here, $\langle u, v\rangle$ denotes the L_2-product of u and v over the boundary Γ, i.e., $\langle u, v\rangle = \int_\Gamma uv\,\mathrm{d}s$. The mass matrix B is thus the discretization of the identity operator $\mathcal{I}$ and the matrix G is the discretization of the operator $\mathcal{G}$. Note that the vector f_N is filled with zeros on the Dirichlet and Robin boundaries, Γ_D and Γ_R, which corresponds to a zero extension of the given datum g_N. Combining Eqs. (24) and (26), yields the system of equations

$$\begin{pmatrix} \mathsf{V} & -\mathsf{K} \\ \mathsf{B} & \mathsf{G} \end{pmatrix} \begin{pmatrix} \mathsf{q} \\ \mathsf{u} \end{pmatrix} = \begin{pmatrix} \mathsf{f}_D \\ \mathsf{f}_N \end{pmatrix}, \tag{28}$$

which is of dimension $(M+N)\times(L+N)$. Obviously, $M = L$ is a necessary condition for the solvability of this system which implies that there have to be as many collocation equations as coefficients q_j. The specific choice of collocation points will be discussed below.

In the dynamic case, the situation is very similar. The spatial approximation is the same as in Eq. (22), i.e.,

$$\begin{aligned} u_{\Gamma,h}(\mathbf{x},t) &= \sum_{i=1}^{N} \varphi_i(\mathbf{x}) u_i(t) \\ q_h(\mathbf{x},t) &= \sum_{j=1}^{M} \psi_j(\mathbf{x}) q_j(t)\,, \end{aligned} \tag{29}$$

with the difference that the coefficients u_i and q_j are still functions of time. Again, the spatial approximation is inserted into the integral Eq. (16) and the resulting residual is collocated on the points $\mathbf{x}^*_\ell$. This yields the semi-discrete set of convolution equations

$$\begin{pmatrix} \mathsf{V}_t & -\mathsf{K}_t \\ \mathsf{B}_t & \mathsf{G}_t \end{pmatrix} * \begin{pmatrix} \mathsf{q}_t \\ \mathsf{u}_t \end{pmatrix} = \begin{pmatrix} \mathsf{f}_{D,t} \\ \mathsf{f}_{N,t} \end{pmatrix}. \tag{30}$$

The matrix entries are now defined by application of the dynamic boundary integral operators to the shape functions but still ignoring the temporal convolution. Hence, they have the same form as in Eq. (25), but all the objects are still functions of time. Moreover, auxiliary matrix operators B_t and G_t have been used in order to allow for the condensed notation in Eq. (30) by setting

$$\mathsf{B}_t[k,j] = \langle \varphi_k, \psi_j \rangle \delta(t) \quad \text{and} \quad \mathsf{G}_t[k,i] = \langle \varphi_k, \varphi_i \gamma \rangle \delta(t)\,. \tag{31}$$

Obviously, it remains to find a suitable temporal discretization for the system of Eqs. (30).

Note that in the above definitions of matrix entries it has been assumed, for simplicity only, that the application of the boundary integral operators is exact. Of course, these integrals will be solved numerically and, therefore, be subject to errors. The quadrature rules for the evaluation of these expressions are discussed in section 4.

Collocation points. As indicated above, one has the necessity of using as many collocation equations as coefficients q_j. Therefore, it is straightforward to place on every element τ_e of the discretization of Γ as many collocation points as shape functions for the unknown q are used on that element. If q is, for instance, approximated by piecewise constant functions, the midpoint of each element seems to be the ideal location for the collocation points. In case of a piecewise linear discontinuous approximation, the situation is more involved. Now, the logical consequence would be to put the collocation points at the vertices of each element. Unfortunately, this makes the collocation equations redundant. Hence, it is preferred to place them in such a manner that they are distributed uniformly in case of a uniform discretization. This implies that the neighbors of each collocation point are as far away as possible. It is chosen here, to use the points $\xi = \pm\frac{1}{2}$ from the reference interval $-1 \leq \xi \leq 1$ of linear line elements for a two-dimensional analysis. On the reference triangle $\hat{\tau} = \{0 \leq \xi_1 \leq 1, 0 \leq \xi_2 \leq 1 - \xi_1\}$ for a three-dimensional analysis, these points are located at $(\frac{1}{6}, \frac{1}{6})$, $(\frac{1}{6}, \frac{2}{3})$, and $(\frac{2}{3}, \frac{1}{6})$. These positions are depicted in Fig. 1. Note that due to the fact that the collocation points are strictly inside the elements the surrounding surface is always smooth. Therefore, the integral-free term simply becomes $\mathcal{C} = \frac{1}{2}\mathcal{I}$. The matrix C which is contained in K has thus the entries

$$\mathsf{C}[\ell, i] = \frac{1}{2}\varphi_i(\mathbf{x}^*_\ell)\,. \tag{32}$$

Obviously, expression (32) is a lot more comfortable as the analytic expressions for the integral-free term derived in [24] for three-dimensional elastostatics. Moreover, in the expressions of [24] material parameters enter. If these are dependent on the Laplace parameter as in the case of the viscoelastic analysis in [35], they have to be recomputed for every Laplace parameter.

Comparison to nodal collocation. The main difference in the presented approach to the classical nodal collocation is the mixed approximation of Eq. (22). In the nodal collocation, one uses exactly the same shape functions for the unknown q as for u_Γ and applies them to the integral Eq. (21). The collocation points are then the nodal coordinates of the spatial discretization. The system of equations is then obtained by assembling the columns of the matrices V and K to the left and right hand sides depending on whether they correspond to an unknown or prescribed coefficient. The application of the Robin boundary conditions is then not so straightforward and

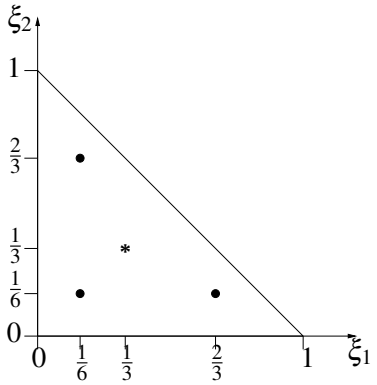

Figure 1: Location of the collocation points for a triangle with a constant shape function (asterisk) or linear shape functions (bullets) for the approximation of q.

requires either additional equations or manipulations of the system matrix [13]. The advantages and disadvantages of the different approaches are outlined in section 7.

3.2 Temporal discretization

In order to convert system (30) into a series of algebraic equations, the occurring convolution integrals have to be solved. The classical way to do so, is to introduce shape functions for the time behavior of the coefficients $u_i(t)$ and $q_j(t)$ and solve the resulting integrals analytically [23, 34]. Here, the convolution quadrature method is used, which yields a quadrature rule for convolution type integrals based on quadrature weights which depend on the Laplace transform of one of the operands. This method goes back to [22] and has been compared with the standard approach in [35]. Whereas the direct approach based on the time-domain fundamental solution U of the operator $\mathcal{H}$ is computationally more efficient, it suffers from severe stability restrictions. For this reason and the possible extension to viscoelastodynamic analyses, the convolution quadrature method based on the Laplace transform fundamental solution $\hat{U}$ is preferred in this work.

Consider, for simplicity, the application of the spatially discretized single layer operator

$$\mathsf{h}(t) = (\mathsf{V}_t * q_t)(t) = \int_0^t \mathsf{V}_t(t-\tau) q_t(\tau)\,\mathrm{d}\tau\,. \tag{33}$$

The value of the resulting vector h at the time instant $t_n = n\Delta t$ of an equidistant time grid is now approximated by the formula

$$\mathsf{h}(t_n) \approx \sum_{\nu=0}^{n} \omega_{n-\nu}(\Delta t, \hat{\mathsf{V}}, \chi)\mathsf{q}_t(\nu\Delta t)\,. \tag{34}$$

In this approximation, the $\omega_{n-\nu}$ are the weights generated by the convolution quadrature method and depend on the size of the time step, the Laplace transform $\hat{\mathsf{V}}$ of the operator matrix V_t, and the characteristic polynomial χ of a suitably chosen multistep method. Here, a BDF2 [20] is

chosen which fulfills all the criteria of the convolution quadrature method [22]. Using now the following notation for $n = 0, 1, \ldots$, and $\nu \leq n$

$$\begin{aligned} \mathsf{V}_{n-\nu} &= \omega_{n-\nu}(\Delta t, \hat{\mathsf{V}}, \chi) \qquad & \mathsf{q}_n &= \mathsf{q}_t(n\Delta t) \\ \mathsf{K}_{n-\nu} &= \omega_{n-\nu}(\Delta t, \hat{\mathsf{K}}, \chi) \qquad & \mathsf{u}_n &= \mathsf{u}_t(n\Delta t)\,, \\ \mathsf{f}_{D,n} &= \mathsf{f}_D(n\Delta t) & \mathsf{f}_{N,n} &= \mathsf{f}_N(n\Delta t) \end{aligned} \tag{35}$$

results in the series of systems of equations

$$\begin{pmatrix} \mathsf{V}_0 & -\mathsf{K}_0 \\ \mathsf{B} & \mathsf{G} \end{pmatrix} \begin{pmatrix} \mathsf{q}_n \\ \mathsf{u}_n \end{pmatrix} = \begin{pmatrix} \mathsf{f}_{D,n} \\ \mathsf{f}_{N,n} \end{pmatrix} - \sum_{\nu=1}^{n} \begin{pmatrix} \mathsf{V}_{n-\nu} & \mathsf{K}_{n-\nu} \\ & \end{pmatrix} \begin{pmatrix} \mathsf{q}_\nu \\ \mathsf{u}_\nu \end{pmatrix}. \tag{36}$$

Note that the matrices B and G are identical with the static case and their coefficients are defined in Eq. (27).

4 Numerical integration

In order to obtain the systems of Eqs. (28) and (36), the application of the respective integral operators has to be carried out numerically. As common in boundary element methods, one has to distinguish between the situation when the collocation point $\mathbf{x}_\ell^*$ is located inside or outside the surface element τ_e on which the integration is carried out. Whereas the former case of improper integrals needs special attention, the latter case of a regular integral can be carried out by means of Gaussian quadrature. Nevertheless, the integrand behaves almost singular if the collocation point is close to the region of integration and, therefore, the regular integration also needs special attention.

4.1 Regular integrals

For sake of simplicity, only the integration on triangles is considered here. Nevertheless, the techniques are easily adapted for quadrilateral elements or for the line integrals of a two-dimensional analysis. An exemplary integral is

$$I(k; \mathbf{x}^*) = \int_0^1 \int_0^{1-\xi_1} k(\mathbf{x}^*, \mathbf{x}(\xi_1, \xi_2))\, \mathrm{d}\xi_2\, \mathrm{d}\xi_1\,, \tag{37}$$

which is obtained after a coordinate transformation from the global coordinates to the reference triangle $\hat{\tau}$. The generic integrand k contains the shape function, the Gram determinant of the coordinate transformation and the fundamental solution or its derivative. The latter is assumed to behave like $|\mathbf{x} - \mathbf{x}_\ell^*|^{-2}$ and, therefore, this distance is the crucial measure of the quality of the numerical integration. In order to compute the distance between collocation and integration point in reference coordinates, at first the coordinates $\xi^* = (\xi_1^*, \xi_2^*, \xi_3^*)$ such that $\mathbf{x}(\xi^*) = \mathbf{x}^*$, have to be computed, where $\mathbf{x}(\xi)$ denotes the coordinate transformation from reference to global coordinates. The geometry approximation is assumed to be linear, i.e., $\mathbf{x}(\xi) = \mathbf{x}_1 + \mathbf{t}_1\xi_1 + \mathbf{t}_2\xi_2 + \mathbf{n}\xi_3$ with the triangle vertices $\mathbf{x}_i$ ($i = 1, 2, 3$), the tangent vectors $\mathbf{t}_1 = \mathbf{x}_2 - \mathbf{x}_1$ and $\mathbf{t}_2 = \mathbf{x}_3 - \mathbf{x}_1$,

and the normal vector $\mathbf{n} = \mathbf{t}_1 \times \mathbf{t}_2$. Then, the reference coordinates of the collocation point can be computed by solving the equation

$$\mathbf{x}_1 + \mathbf{t}_1\xi_1^* + \mathbf{t}\xi_2^* + \mathbf{n}\xi_3^* = \mathbf{x}^* \quad \Rightarrow \quad \mathsf{M}\xi^* = \mathbf{x}^* - \mathbf{x}_1\,, \tag{38}$$

where the matrix M is composed of the tangent and normal vectors, $\mathsf{M} = [\mathbf{t}_1, \mathbf{t}_2, \mathbf{n}]$. In general, the tangent vectors $\mathbf{t}_1$ and $\mathbf{t}_2$ are not mutually orthogonal. But, by definition, the normal vector $\mathbf{n}$ is orthogonal to the plane spanned by the tangent vectors. Therefore, by multiplication with $\mathbf{n}$, the value of ξ_3^* is easily computed and equation (38) reduces to a 2×2-system which is solved easily.

In view of the final criterion for the quality of the quadrature, the minimal distance r between the reference triangle $\hat{\tau}$ and the coordinates ξ^* has to be computed. This is easily done by detecting the point $\hat{\xi} \in \hat{\tau}$ which lies closest to ξ^* and setting $r = |\hat{\xi} - \xi^*|$.

Once these geometrical entities are computed, the error estimate of [19]

$$|E_p| < C\frac{1}{2^p}\frac{1}{r^{p+2}} \tag{39}$$

is used, where C is some constant and p is the maximal order of a polynomial which is integrated exactly by the quadrature rule. For Gauß-Legendre quadrature in one dimension, one has the well-known result $p = 2n_g + 1$ with n_g denoting the number of evaluation points the rule is using [17]. For other quadrature rules, e.g., the triangle rules of [9], which are used here for a three-dimensional analysis, the order p is usually a given quantity associated with the rule. E_p is the error of that rule of order p and is a prescribed value. Taking the logarithm of expression (39), yields a rule for the order p

$$p \leftarrow 2\left\lceil \frac{\log(C) - \log|E_p| - \log(r^2)}{\log(4r^2)} \right\rceil \tag{40}$$

under the assumption that $\log(4r^2)$ is greater than zero. $\lceil x \rceil$ denotes here the smallest integer greater than or equal to x.

If the order p computed according to the rule (40) is greater than some value p_{max} of the highest quadrature rule available or the condition $\log(4r^2) > 0$ is violated, the triangle $\hat{\tau}$ is subdivided into four sub-triangles. The numerical integration is then carried out on each of these sub-triangles with an order $p_{\max}$ unless a further subdivision is necessary. Hence, a recursive scheme is started in which on each sub-triangle the rule (40) is recomputed with a new value of the minimal distance r, now with respect to the considered sub-triangle, and a new tolerance which is reduced according to the area of the sub-triangle. This recursion takes place until $p \leq p_{max}$ or a maximal level of recursion is reached.

Note that Eq. (39) is not understood as a sharp error estimate but rather an expression which grasps the asymptotic behavior of the integrand. It only refers to the monomial of r with the highest order and, moreover, it neglects the influence of the shape function and the Gram determinant on the integrand.

4.2 Singular integration

Here, the collocation point is located *inside* the element of integration, i.e., $\mathbf{x}_\ell^* \in \tau_e$. Therefore, the integral kernels of the single and double layer operators, $\mathcal{V}$ and $\mathcal{K}$ (or $\mathcal{V}_t$ and $\mathcal{K}_t$ for the

dynamics case), tend to infinity as $|\mathbf{y}-\mathbf{x}^*| \to 0$. Whereas the integral kernels of the scalar models (Laplace's equation and scalar wave equation) and the single layer operators of the vector models (elastostatics and elastodynamics) are weakly singular, the double layer operator of the vector models is only defined in the sense of a Cauchy principal value integration [17]. The treatment of such integral is described in the following subsection 4.3. For the time being, only weakly singular integrals are considered.

A common approach to handle singular integrals in the context of boundary element methods, is to subtract the leading singularity which can then be treated by analytical techniques or special quadrature rules. The difference term, i.e., integral kernel minus leading singularity, is thus a regular function. Nevertheless, this regularity only refers to the term itself but not to any higher order derivative. But these derivatives determine the quadrature error [17]. Consider, for instance, the Bessel function $K_0(x)$ which occurs in the fundamental solutions of the Laplace transformed scalar wave equation or elastodynamics. This function has a leading singularity of $-\log(x)$. The standard approach would be to use a logarithmic quadrature rule [31] for the logarithmic singularity and then a standard Gaussian quadrature for the term $K_0(x)+\log(x)$. But the derivatives of this difference term are again singular and, therefore, the quadrature error cannot be controlled. Due to this observation, it is desirable to have a quadrature rule which is applicable to the integral kernel as a whole.

In the three-dimensional analysis, the weakly singular integrals over surface triangles are carried out by the rules developed in [19]. This approach is also known as Duffy coordinates [8] in the mathematical community. The only difference here is that the point of singularity is not located on a vertex but inside the element. Therefore, by drawing lines to the vertices and dropping perpendiculars on the sides, the triangle is subdivided into six triangular regions of integration where each one has the singularity on a vertex. Alternatively, one could also use polar coordinates. Confer [10] for a comparison and [37] for an in-depth mathematical analysis of these two approaches.

For the weakly singular line integrals in two-dimensional analyses the semi-sigmoidal transformations due to [15] are used. These transformations work in the same black-box fashion as Duffy coordinates by mapping the region of integration onto itself with a non-linear coordinate transformation which yields a Jacobian alleviating the singularity.

4.3 Regularization

The double layer operator of the elastostatic and elastodynamic equations is only defined in the sense of a Cauchy principal value. Therefore, suitable quadrature rules which can be used in the desired black-box fashion are not easily constructed. For this reason, it is here preferred to apply an analytical technique which yields a weakly singular representation. Such techniques are commonly referred to as *regularization*.

A regularized expression of the elastostatic double layer operator is given by [18] and has the

form (see also [25, 41])

$$\begin{aligned}(\mathcal{K}^E u_\Gamma)(\mathbf{x}) = &-\frac{1}{2(d-1)\pi}\int_\Gamma u_\Gamma(\mathbf{y})\frac{(\mathbf{y}-\mathbf{x})\cdot\mathbf{n}(\mathbf{y})}{|\mathbf{y}-\mathbf{x}|^d}\,\mathrm{d}s_\mathbf{y}\\ &-\frac{1}{2(d-1)\pi}\int_\Gamma E(\mathbf{x}-\mathbf{y})(\mathcal{M}_\mathbf{y} u_\Gamma)(\mathbf{y})\,\mathrm{d}s_\mathbf{y}\\ &+2\mu(\mathcal{V}^E(\mathcal{M}_\mathbf{y} u_\Gamma))(\mathbf{x})\,.\end{aligned} \tag{41}$$

Recall that $d = 2,3$ is the dimension of the problem and $\mathbf{n}$ the unit outward normal vector. The function $E(\mathbf{x})$ is either $E(\mathbf{x}) = -\log|\mathbf{x}|$ or $E(\mathbf{x}) = 1/|\mathbf{x}|$ for the cases $d = 2$ or $d = 3$, respectively. The operator $\mathcal{M}_\mathbf{y}$ appearing in Eq. (41) is referred to as Günther derivative [18] and has the components

$$\mathcal{M}_\mathbf{y}[i,j] = n_j(\mathbf{y})\frac{\partial}{\partial y_i} - n_i(\mathbf{y})\frac{\partial}{\partial y_j}\,, \tag{42}$$

where y_i is the i-th component direction of the position vector $\mathbf{y}$ and n_i is the i-th component of the normal vector $\mathbf{n}(\mathbf{y})$ located at the boundary point $\mathbf{y}$. A derivation and alternative representations of Eq. (42) are given in [41]. Expression (41) is composed of three parts, the double layer operator of Laplace's equation and the single layer operators of Laplace's equation and Elastostatics. The latter two are not applied to the function u_Γ itself but to special derivatives of it with the operation due to Eq. (42). All three integral operators are now weakly singular and the application of $\mathcal{M}_\mathbf{y}$ is well defined because the test functions used for the approximation of u_Γ, see Eq. (22), are continuous.

In the remaining case of elastodynamics, an expression similar to Eq. (41) can be derived and is given in [16] for the three-dimensional case. The transfer to two dimensions is straightforward and not repeated here. Note that in the derivation of these regularizations, the boundary Γ is assumed to be a closed surface such that $\partial\Gamma = \emptyset$ holds, i.e., the surface itself has no boundary. For some applications, e.g., the discretization of an elastic halfspace by a surface patch, this assumption is violated.

5 Solution of the systems

Due to the spatial and temporal discretizations as presented in subsections 3.1 and 3.2, the systems of Eqs. (28) and (36) are obtained. The block matrix of both systems has exactly the same structure. But in the dynamic case, system (36) has to be solved repeatedly for different right hand sides. Therefore, a direct solver can be still advantageous and is considered here. For simplicity, only system (28) is considered in the following.

A static condensation of the system of Eqs. (28) gives the reduced system of equations

$$\mathsf{S}\mathsf{u} = \mathsf{g}\,, \tag{43}$$

where $\mathsf{S} = \mathsf{G} + \mathsf{B}\mathsf{V}^{-1}\mathsf{K}$ and $\mathsf{g} = \mathsf{f}_N - \mathsf{B}\mathsf{V}^{-1}\mathsf{f}_D$. Using LU-factorizations [11] instead of computing the inverse of V, yields the following steps

$$\begin{aligned}\mathsf{L}_V\mathsf{U}_V &= \mathsf{V} \qquad & \mathsf{L}_V\mathsf{U}_K &= \mathsf{K}\\ \mathsf{L}_B\mathsf{U}_V &= \mathsf{B} & \mathsf{S} &= \mathsf{G} + \mathsf{L}_B\mathsf{U}_K\,,\end{aligned} \tag{44}$$

which are one LU-factorization, two forward-backward substitutions, and one matrix-matrix multiplication. The right hand side g is computed by similar operations. The solution of system (43) is then another LU-solve. Once the coefficients u are known, the vector q is easily computed. The solution steps (44) can be carried out by any linear algebra package, e.g., [2]. It has to be noted that the use of pivotization might be necessary and, therefore, these steps need additional column and row interchanges which are not outlined here.

Stability problem. Assume now that $\mathsf{G} = 0$, i.e., that no Robin boundary conditions are prescribed because this situation corresponds to the worst case scenario. As outlined in [39], the type of approximation used in Eq. (22) is crucial for the stable solution of system (28). The basic conditions for the invertibility of the considered system are the existence of the inverses V^{-1} and S^{-1} [4]. Whereas the existence of V^{-1} is assumed based on the theoretical knowledge that $\mathcal{V}$ is an elliptic operator and the experience that collocation methods in combination with conforming discretizations work. The existence of S^{-1} is rather tricky and two necessary conditions are considered.

At first $M > N$ is postulated, i.e., there have to be more coefficients q_j than u_i. The other condition is that the matrices K and B have full rank, i.e., $\operatorname{rank}(\mathsf{K}) = \operatorname{rank}(\mathsf{B}) = N$. Both conditions can be fulfilled by either choosing a finer mesh for the approximation of q or by using equal order approximations [39]. The latter option is considered here and implies that, for instance, piecewise linear continuous trial functions are used for $u_{\Gamma,h}$ and piecewise linear discontinuous functions for q_h. Unfortunately, the rank condition rules out the use of piecewise constant shape functions for q_h which would be a natural choice with less degrees of freedom.

6 Numerical results

6.1 Bar problem

Consider the one-dimensional problem depicted in Fig. 2, where a bar of length ℓ is fixed at its left end and loaded at its right end. In terms of an elastic model, the displacement field is prescribed with zero at $x_1 = 0$ and the surface traction is given as $q = F$ at $x_1 = \ell$. In dynamics, the applied force term F is assumed to behave like $F(t) = F_0 H(t)$ in time with $H(t)$ denoting the Heaviside or unit step function.

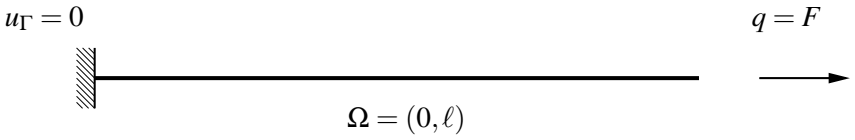

Figure 2: Bar subject to axial force.

The physical interpretations of this problem are either a column of an acoustic fluid subject to a specific surface flux or the already mentioned elastic bar with an applied traction. In the former case, the material parameters are assumed as $\kappa = 1.42 \cdot 10^5\,\mathrm{N/m^2}$ and $\rho = 1.2\,\mathrm{kg/m^3}$ for the compressibility modulus and the mass density of the acoustic fluid, respectively. The elastic solid has the Lamé parameters $\lambda = 0$ and $\mu = 1.06 \cdot 10^{11}\,\mathrm{N/m^2}$ and a mass density of $\rho = 7\,850\,\mathrm{kg/m^3}$.

A three-dimensional cuboid of dimension $3 \times 1 \times 1\,\mathrm{m}$ is used for the representation of this problem which is discretized by surface triangles of three different sizes. The shorter side lengths of these triangles are taken as $h = 0.5\,\mathrm{m}$, $0.25\,\mathrm{m}$, and $0.2\,\mathrm{m}$ which yields 112, 448, and 700 triangles, respectively. The different meshes are depicted in Fig. 3.

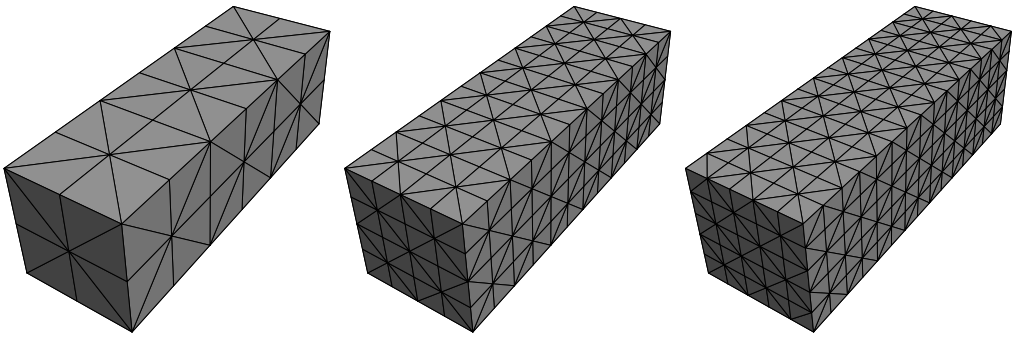

(a) $h = 0.5\,\mathrm{m}$ (b) $h = 0.25\,\mathrm{m}$ (c) $h = 0.2\,\mathrm{m}$

Figure 3: Different spatial discretizations.

The temporal discretization is carried out as described in subsection 3.2. The size of the time steps Δt are then chosen such that the CFL-number [7]

$$\beta = \frac{c_1 \Delta t}{h} \tag{45}$$

has specific values, where c_1 denotes the velocity of the compression wave. For the acoustic fluid it becomes $c_1^2 = \kappa/\rho$ and $c_1^2 = (\lambda + 2\mu)/\rho$ for the elastic solid.

Condition numbers. In the following, the condition numbers of the system matrices for the proposed method are compared with the condition numbers of the nodal collocation. The condition number $\mathrm{cond}(\mathsf{A})$ is measured in the one-norm, i.e., $\mathrm{cond}(\mathsf{A}) = \|\mathsf{A}\|_1 \|\mathsf{A}^{-1}\|_1$. In fact, the condition number estimate of LAPACK [2] is used which is based on the algorithm of [14]. Let A be the system matrix obtained by nodal collocation. V denotes the upper left block matrix of system (28) or (36) for the static or the dynamics case, respectively. Furthermore, S is the Schur complement obtained by static condensation as given in Eq. (43). The dimensions of these matrices are given in Tab. 1 for the three different meshes and the two considered materials.

In Tab. 2, the respective condition numbers for the Laplace equation (fluid) and elastostatics (solid) are given for the three different meshes. It has to be noted that the matrix A is assembled after a variable transformation in which the geometry and the material parameters are scaled to achieve a better condition number (see [36] for details on this scaling). Without this variable transformation, the number $\mathrm{cond}(\mathsf{A})$ would be totally out of bound. Comparing the numbers of Tab. 2, it becomes clear that the condition numbers of A, V, and S are of comparable magnitudes for Laplace equation. But in the case of elastostatics, V is still well-conditioned, whereas the matrices A and S have condition numbers about on order of magnitude greater with $\mathrm{cond}(\mathsf{A}) < \mathrm{cond}(\mathsf{S})$.

	mesh	dim(A)	dim(V)	dim(S)
fluid	a	58	336	49
	b	226	1 344	201
	c	352	2 100	316
solid	a	174	1 008	147
	b	678	4 032	603
	c	1 056	6 300	948

Table 1: Dimensions of the system matrices for different meshes.

	mesh	cond(A)	cond(V)	cond(S)
fluid	a	215	137	132
	b	352	277	240
	c	716	344	343
solid	a	4 100	207	5 761
	b	7 740	420	11 695
	c	8 048	550	16 180

Table 2: Condition numbers for the static computations.

(a) fluid

mesh	a	a	a	b	b	b	c	c	c
β	0.2	0.4	0.8	0.2	0.4	0.8	0.2	0.4	0.8
cond(A)	75.1	51.1	46.4	153	101	86.0	625	413	351
cond(V)	7.49	14.7	28.3	7.71	13.1	25.9	4.33	7.98	16.7
cond(S)	8.43	7.06	5.89	8.74	7.23	5.46	9.08	8.90	8.25

(b) solid

mesh	a	a	a	b	b	b	c	c	c
β	0.2	0.4	0.8	0.2	0.4	0.8	0.2	0.4	0.8
cond(A)	267	187	181	540	353	311	705	463	417
cond(V)	9.32	15.2	30.9	9.19	16.1	28.4	5.66	9.50	16.8
cond(S)	13.1	14.8	17.4	12.0	14.3	15.9	13.8	15.4	23.6

Table 3: Condition numbers for the dynamic computations.

In Tab. 3, the condition number for the dynamic cases are given, where the three meshes with three different time step sizes are compared. The time steps are such that the CFL-number has the values $\beta = 0.2$, $\beta = 0.4$, and $\beta = 0.8$. The results for the scalar wave equation are shown in Tab. 2(a) and the Tab. 2(b) gives the values for the elastodynamics system.

In the dynamic case, the condition numbers cond(A) are significantly larger than cond(V) and cond(S). Moreover, the asymptotic behavior of these condition numbers differs for the compared methods. The number cond(A) gets large with more degrees of freedom and smaller for increasing time steps. On the contrary, the condition number of the single layer matrix cond(V) becomes smaller for finer meshes and larger for bigger time steps. The behavior of cond(S), the condition number of the Schur complement, is not so easily described. In most cases, it becomes slightly bigger with an increase of degrees of freedom. But if the time step is increased, it gets smaller in the fluid case and larger in the solid case.

Accuracy and stability. The considered one-dimensional problem has an analytical solution which is derived in [12], see also [34]. In order to compare the quality of the numerical results, this analytical solution is used as a reference. The outcome of an elastodynamic solution of the considered problem is shown in Fig. 4, where the longitudinal displacement component u_1 is considered at the right end $x_1 = \ell$ in Fig. 4(a) and the surface traction q_1 at the left end $x_1 = 0$ in Fig. 4(b). The computation has been carried out for the coarsest mesh with $h = 0.5\,\mathrm{m}$ only and a time step size such that $\beta = 0.2$. In the figures, *old* refers to nodal collocation and *new* to the here proposed method without being judgemental.

Comparing the displacement results of the different collocation approaches in Fig. 4(a), one can see that the proposed method has less damping of the amplitudes. Moreover, the initial

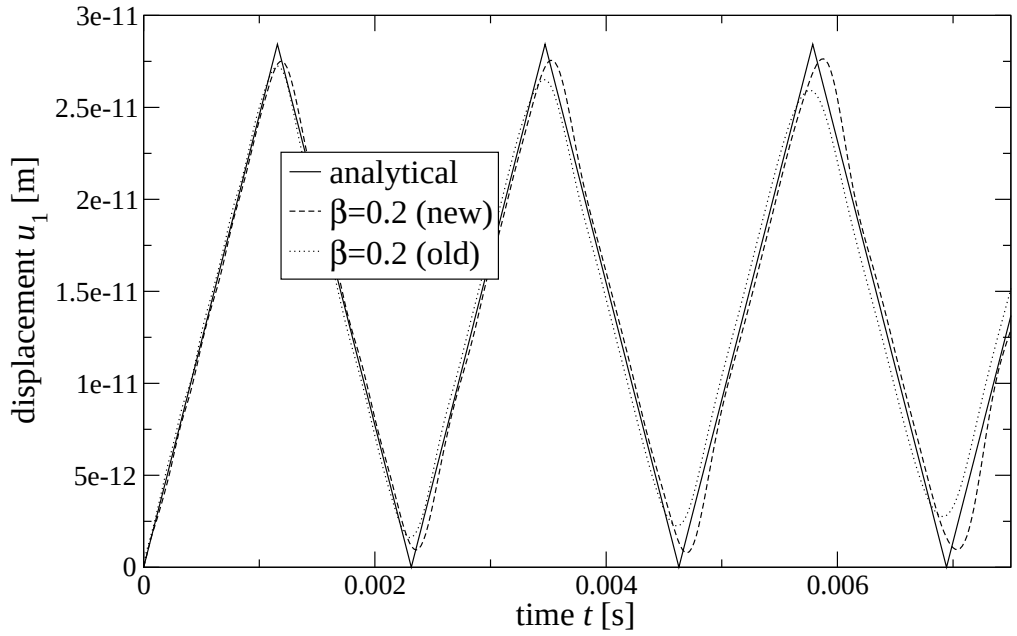

(a) Displacements

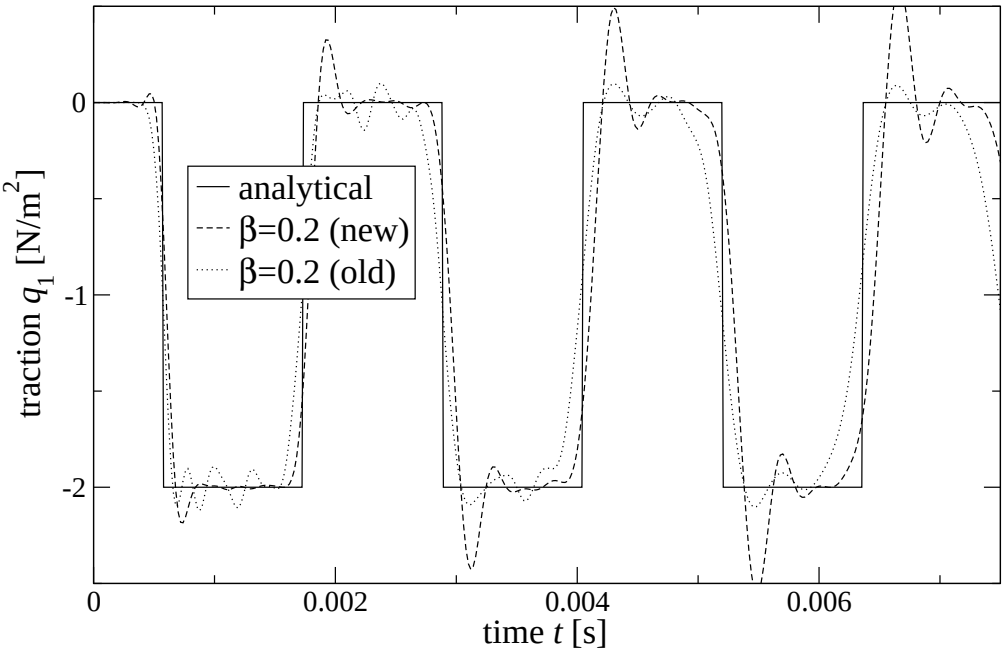

(b) Tractions

Figure 4: Elastodynamic solution of the bar problem.

elongation is already slightly closer to the analytical curve. In view of the traction results in Fig. 4(b), the outcome of the new approach gets closer to the jumps of the piecewise constant analytical solution. This in turn justifies the larger overshoots after these jumps.

Finally, the behavior of the two compared approaches is considered for a smaller time step such that $\beta = 0.1$. The results are shown together with the analytical solution in Fig. 5. In order to emphasize the different stability behaviors, the time range $0.2\,\mathrm{s} < t < 0.8\,\mathrm{s}$ is not plotted. Only the beginning and the end of the computed time period are displayed. Clearly, the displacement solution given in Fig. 5(a) gets out of bound after only a short time period for the nodal collocation, whereas the outcome of the proposed approach remains stable and close to the analytical curve for a significantly larger simulation time. The same phenomenon can be observed for the traction solution of Fig. 5(b), where the nodal collocation fails almost immediately but the new approach yields a curve which slowly builds up.

6.2 Elastic halfspace

Consider now the halfspace Ω^+ with its boundary Γ^+ defined by

$$\begin{aligned} \Omega^+ &= \{\mathbf{x} \in \mathbb{R}^3 : x_3 > 0\} \\ \Gamma^+ &= \{\mathbf{x} \in \mathbb{R}^3 : x_3 = 0\}, \end{aligned} \tag{46}$$

which is occupied by an elastic medium with the properties $\rho = 1884\,\mathrm{kg/m^3}$ and $\lambda = \mu = 1.363 \cdot 10^8\,\mathrm{N/m^2}$. Analytical solutions are available for a point load on the surface in x_3-direction. In the static case, the solution is the halfspace fundamental solution due to Boussinesq, see [21]. A dynamic solution is given by [30] for the surface displacements for a point load varying as a step function in time, i.e., $F(t) = F_0 H(t)$.

The surface Γ^+ defined in Eq. (46) is obviously unbounded. The boundary element discretizations used here are thus surface patches $\Gamma_h^+ \subsetneq \Gamma^+$ which cover only the area around the applied point load. The load itself is represented by a constant traction on some triangles.

Static case. The discretization used for the static case is shown in Fig. 6 and consists of 3200 linear triangles covering an area of $5 \times 5\,\mathrm{m}$. Each triangle has legs of length $0.125\,\mathrm{m}$. Four triangles in the middle of the discretization are subject to a constant vertical traction field g_N such that $F = \int_{\Gamma_h^+} g_N \,\mathrm{d}\mathbf{x} = 1\,\mathrm{N}$. The loaded area is dark shaded in Fig. 6.

The outcome of the boundary element simulations is shown in Fig. 7 together with the Boussinesq solution [21]. In Fig. 7(a), the horizontal displacements are plotted along a horizontal coordinate line through the point of the applied load. Fig. 7(b) shows the vertical displacements along the same line. Since the point load is represented by an area load, the singularity of the analytical solution cannot be reproduced exactly. Nevertheless, the outcome of the new approach has higher peaks and is therefore closer to the analytical curve. In the range of $0.5\,\mathrm{m} < |x_1| < 2\,\mathrm{m}$, the results of both collocation methods are fairly close to the reference solution. On the other hand, close to the edges at $2\,\mathrm{m} < |x_1| < 2.5\,\mathrm{m}$ the results of the nodal collocation deviate significantly from the reference curves, especially for the horizontal displacements u_1.

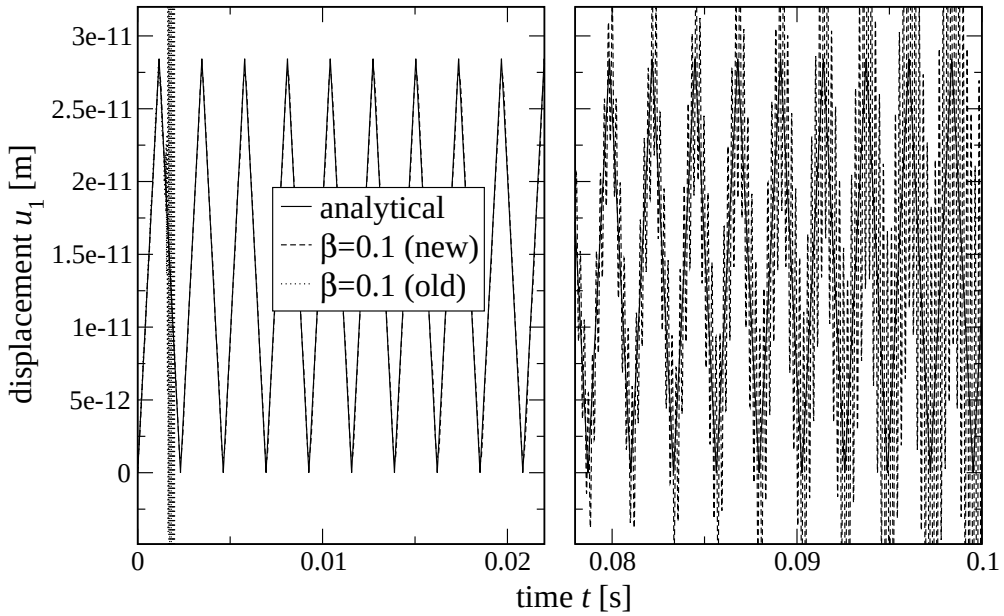

(a) Displacements

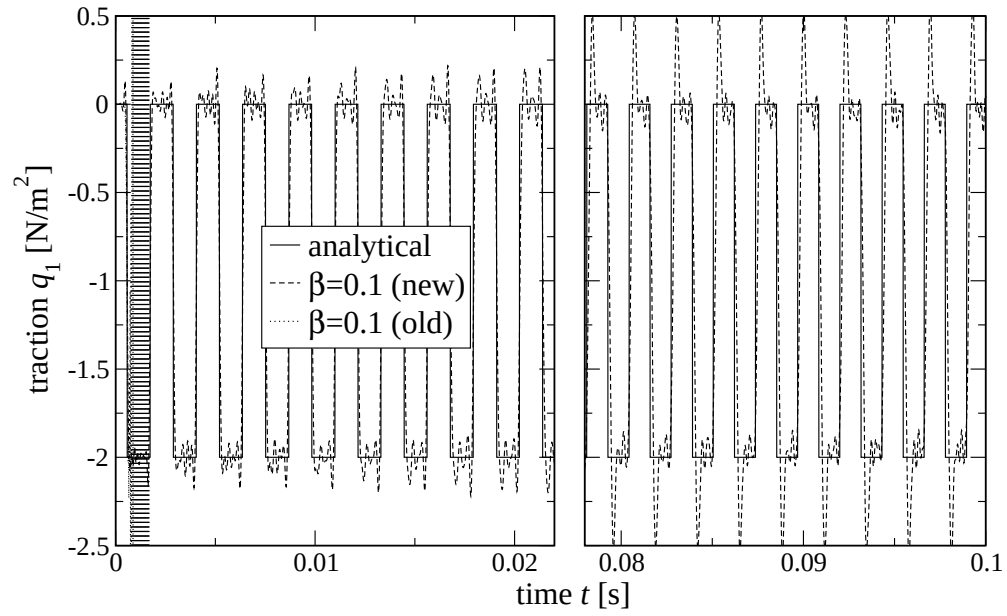

(b) Tractions

Figure 5: Stability behavior of the elastodynamic solution of the bar problem.

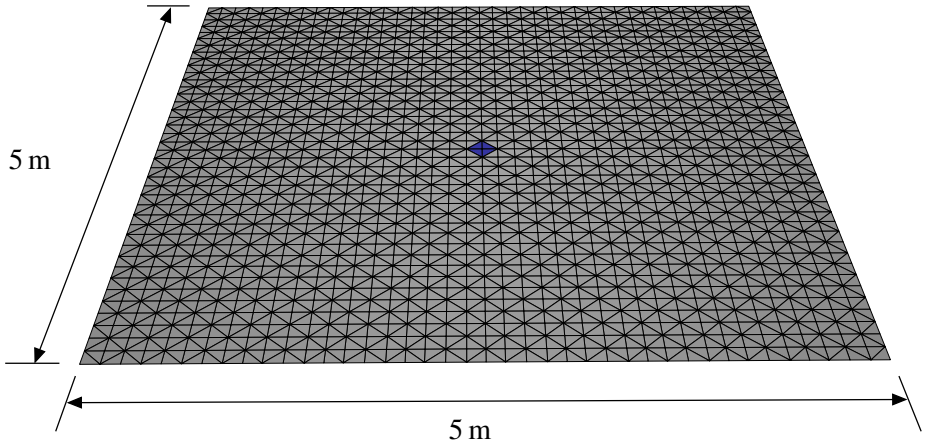

Figure 6: Surface discretization for the elastostatic halfspace.

Dynamic case. Now, the applied point force varies as a unit step function in time and the halfspace reacts dynamically. Fig. 8 shows the used discretization which consists of 396 linear triangles covering an area of dimension $33 \times 6\,\mathrm{m}$. Two triangles (dark shaded in the figure) are subject to a vertical constant traction field g_N such that the net force is $F_0 = 1\,\mathrm{kN}$. The simulations are using a time step size of $\Delta t = 7 \cdot 10^{-4}\,\mathrm{s}$ such that the CFL-number is approximately $\beta = 0.32$ if the length of the legs of the triangles of 1 m is used. At a distance of 15 m from the applied load, the observation point is located for which the computed and analytical solutions are considered.

In Fig. 9, the numerical outcome of the dynamic halfspace problem is shown together with the analytical solution due to [30]. Again, horizontal and vertical displacements are considered in Figs. 9(a) and 9(b), respectively. From the analytical curve, one can clearly see the arrival of the compression wave and the very prominent Rayleigh surface wave, whereas the shear wave is not very distinct. The final asymptote corresponds to the static solution discussed in the previous paragraph. Both numerical solutions show the compression wave and somehow mimic the Rayleigh wave. The peak of the Rayleigh wave is higher for the new approach then in case of the nodal collocation. In turn, this peak produces a higher overshoot for the vertical displacements. In both simulations, the long-time behavior deviates significantly from the static solution. In addition, the outcome of the new approach is polluted by artificial wave reflections. These reflections also occur in the compared nodal collocation but less severely. It can be assumed that these strong reflections are caused by the regularization of the double layer operator, given in Eq. (41). This expression is based on the assumption that the boundary Γ is a closed surface which is violated in the considered case of the halfspace. Nevertheless, the computed solution remains stable and the magnitudes of these wave reflections diminish.

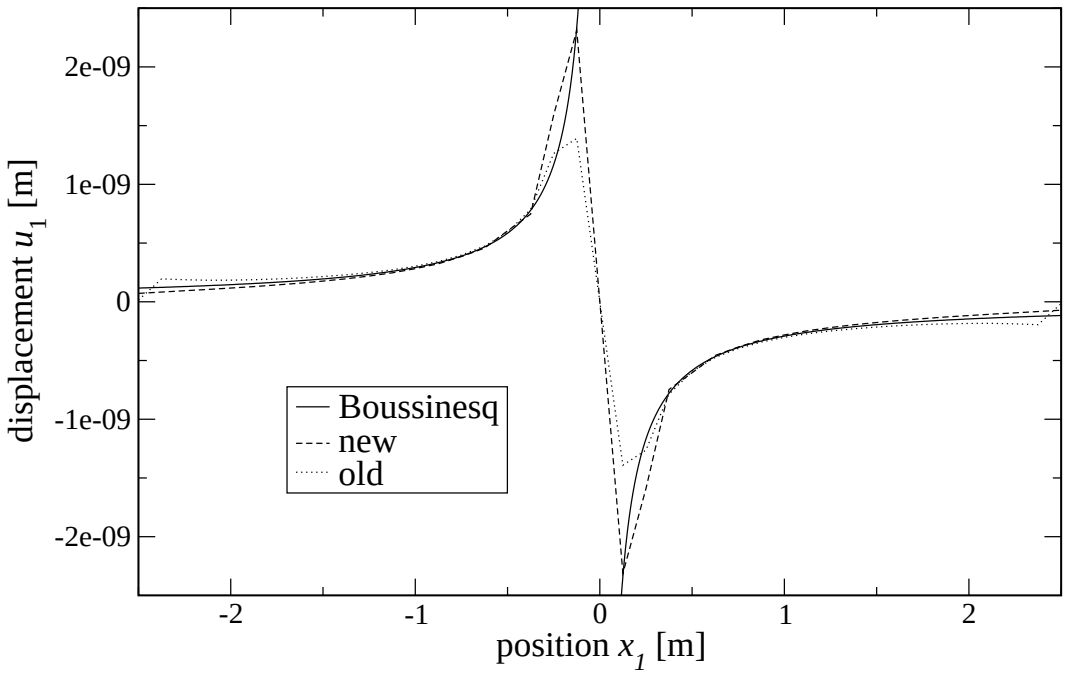

(a) Horizontal displacements

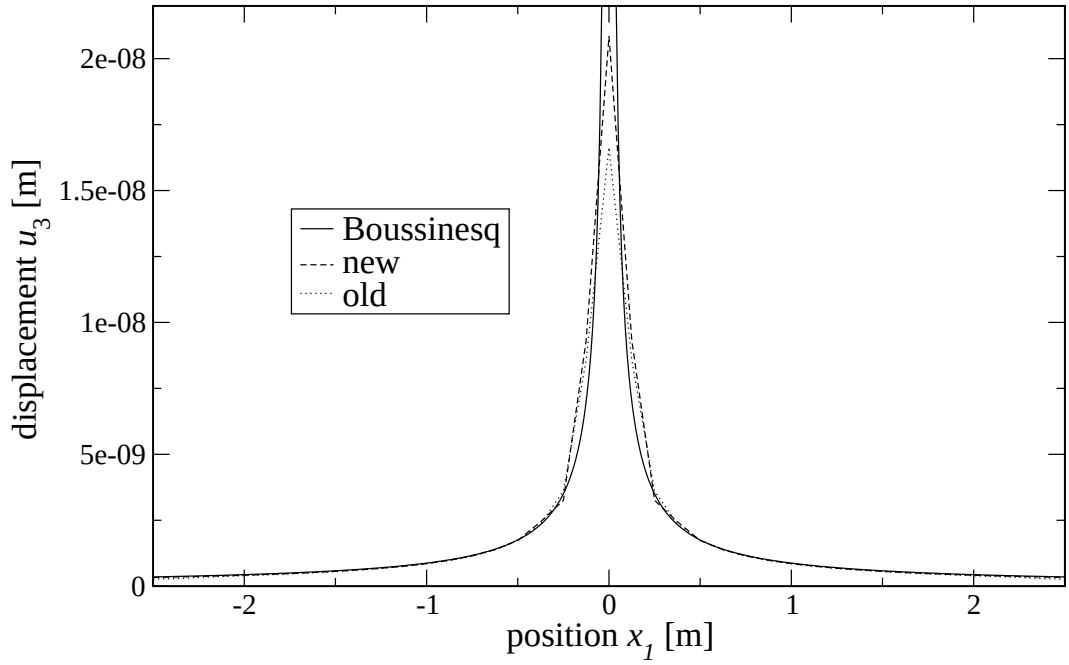

(b) Vertical displacements

Figure 7: Analytical and computed solution of the elastostatic halfspace.

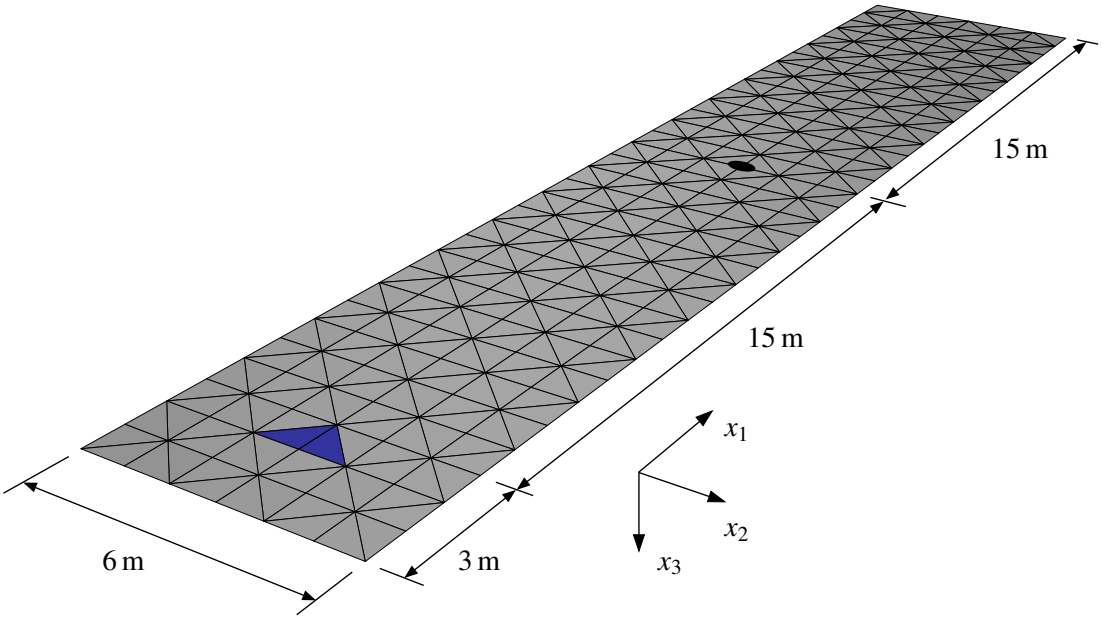

Figure 8: Surface discretization for the elastodynamic halfspace.

6.3 Beam on elastic foundation

At last, a finite beam subject to a point force and continuously bedded on an elastic foundation is considered. The problem is depicted in Fig. 10, where a beam with bending stiffness EI of length ℓ is located on a foundation with bedding modulus k and subject to a vertical point load in its middle.

Using Bernoulli beam theory, the analytical solution of the homogeneous problem is of the form

$$\begin{aligned} w(x) &= \exp(-\tilde{x})(C_1\cos(\tilde{x}) + C_2\sin(\tilde{x})) \\ &\quad + \exp(\tilde{x})(C_3\cos(\tilde{x}) + C_4\sin(\tilde{x})) \quad \text{with} \quad \tilde{x} = x/\lambda\,. \end{aligned} \tag{47}$$

Considering, for instance, only the right half of the problem with the coordinate $0 \le x \le \ell/2$, the constants C_i can be easily obtained by using the boundary conditions $w'(0) = 0$, $w'''(0) = -F/2EI$, $w''(\ell/2) = 0$, and $w'''(\ell/2) = 0$. These conditions represent in order the horizontal tangent in the axis of symmetry, half of the applied point force, no shear force and no bending moment at the free end.

A three-dimensional boundary element analysis is carried out where a cuboid of dimension $10 \times 1 \times 1\,\mathrm{m}$ is used as a representation of the beam. Hence, the moment of inertia is $I = 1/12\,\mathrm{m}^4$. The applied load has the magnitude $F = 10^4\,\mathrm{N}$ and the Young's modulus is taken as $E = 10^6\,\mathrm{N/m^2}$. The function γ of the boundary value problem (2) has the constant value $\gamma = 10^5\,\mathrm{N/m^3}$. Therefore, the bedding modulus of the beam is $k = \gamma b = 10^5\,\mathrm{N/m^2}$, where $b = 1\,\mathrm{m}$ denotes the width of the beam.

The three-dimensional domain is discretized uniformly by linear surface triangles. Two different discretizations are considered with mesh widths $h = 1/2\,\mathrm{m}$ and $h = 1/4\,\mathrm{m}$ which correspond

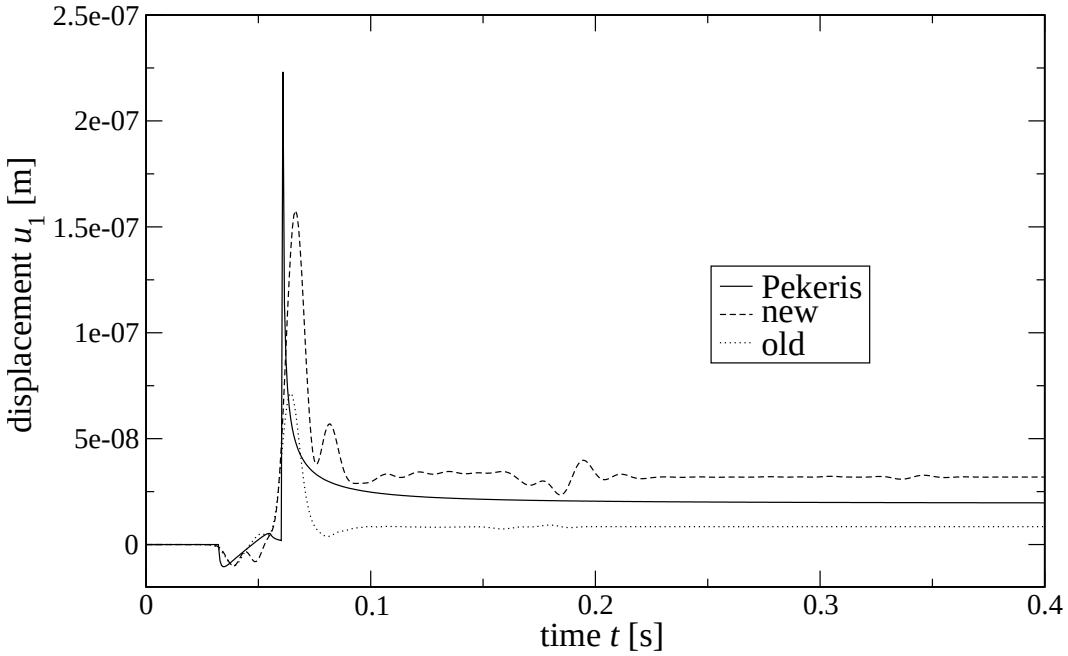

(a) Horizontal displacements

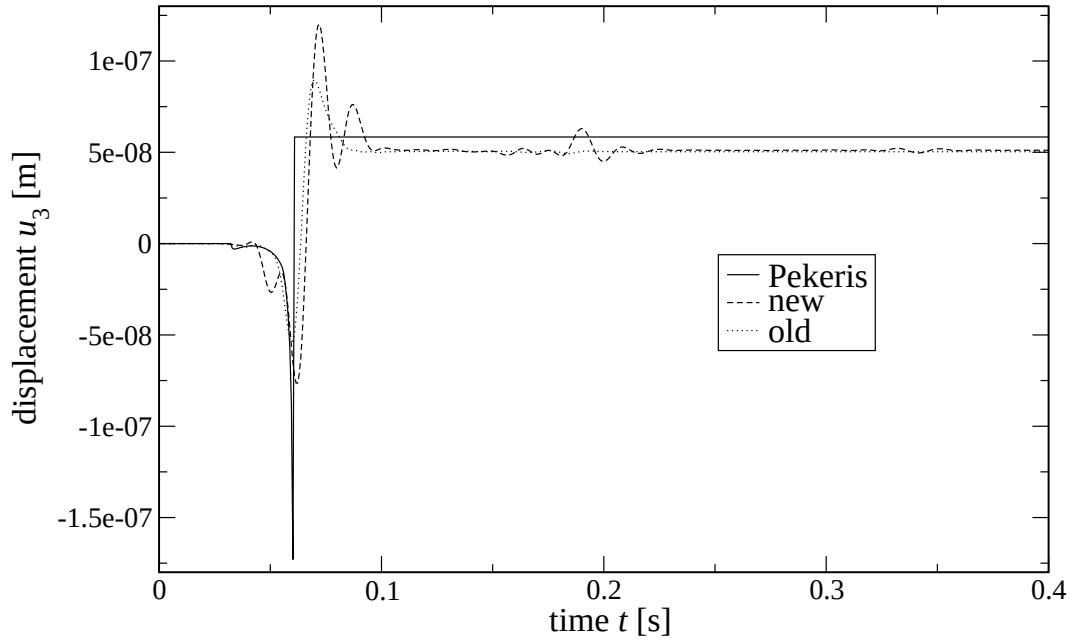

(b) Vertical displacements

Figure 9: Analytical and computed solutions of the elastodynamic halfspace at the observation point.

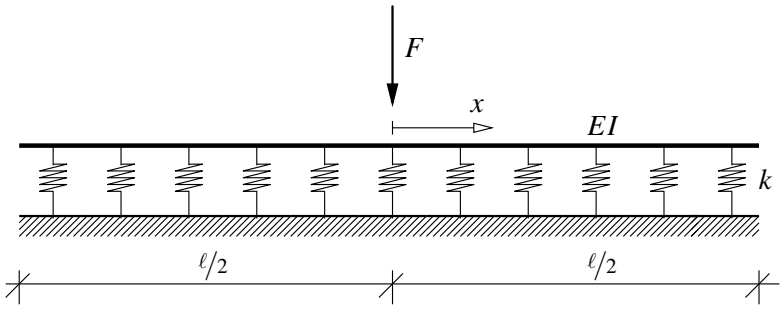

Figure 10: Continuously bedded beam.

to 336 and 1344 elements. An area of $1\,\mathrm{m}^2$ on the top side and in the middle of the cuboid has been loaded constantly such that the net force is $F = 10^4\,\mathrm{N}$. The outcome of the analysis is shown in terms of the line of deflection in Fig. 11 where the terms coarse and fine refer to the larger and small mesh width, respectively. The line of deflection of the numerical analysis is the coordinate line at the bottom surface of the beam. The results of Fig. 11 indicate a good agreement with the reference solution for both the coarse and the fine mesh. Clearly, there are small deviations close to the applied surface load where the compared theories of the Bernoulli beam and the elastic continuum have to differ.

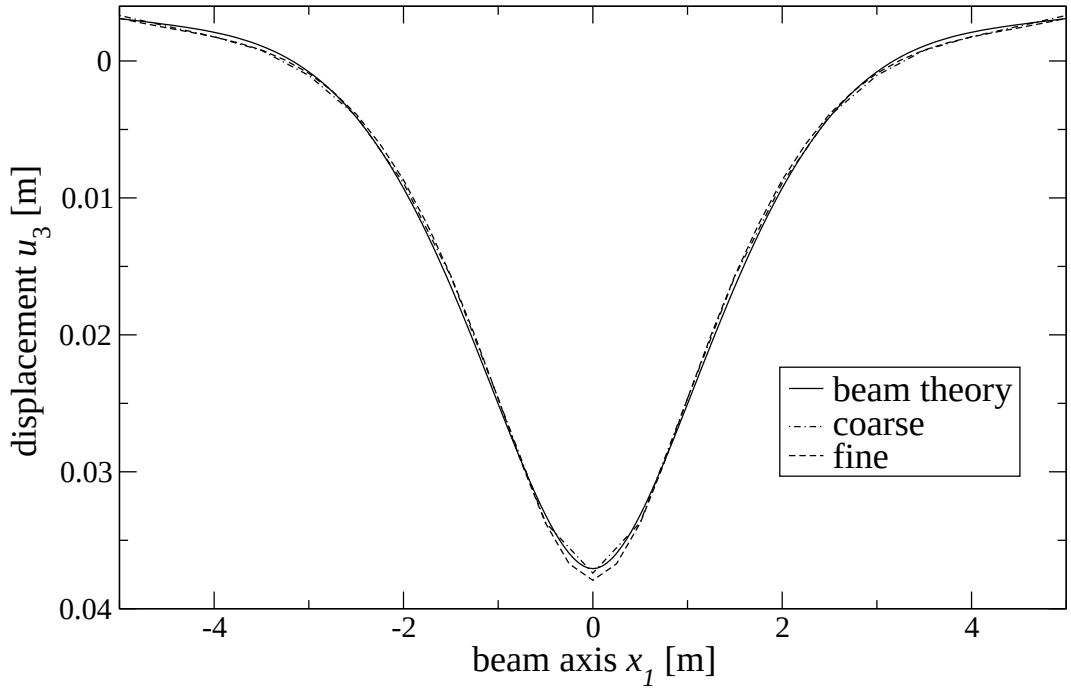

Figure 11: Numerical solution of the beam on elastic foundation with reference solution.

7 Discussion of the method

In this work, a collocation formulation is presented which is based on a mixed approximation (22) similar to the Galerkin scheme of [39]. This approach is applicable to scalar and vector problems of static and dynamic kind. In the following, some remarks on the respective advantages and disadvantages are given.

Due to the mixed approximation orders, the quantities u_Γ (e.g., the surface displacements) and q (tractions) are approximated according to the mathematical spaces they are defined in (cf., e.g., [41] for details). Whereas u_Γ is a continuous quantity and is thus approximated by globally continuous functions, the datum q is defined with respect to the local normal vector. Therefore, q is naturally discontinuous because the computational geometry can have corners and edges. For the same reason, this quantity cannot be unique at these points. These properties are represented by a discontinuous approximation. The use of discontinuous shape functions is discussed in [26], where the loss of uniqueness at corners is used in order to justify these shape functions. Unfortunately, the approach in [26] uses an isoparametric approach such that u_Γ *and* q are approximated by discontinuous shape functions.

This new collocation scheme is tailored to yield a square matrix V as the discretization of the single layer operator $\mathcal{V}$. Since $\mathcal{V}$ is generally known to be elliptic [41], its discretization with Galerkin schemes results in symmetric positive definite system matrices. The presented collocation destroys this symmetry but numerical experiments affirm that V is still positive definite. In view of iterative solution algorithms this property might be useful. Nevertheless, it guarantees that V is invertible. Moreover, the condition numbers of this matrix are very small and seem to be of order $\mathcal{O}(h^{-1})$ as it can be deduced from the analysis in subsection 6.1. The collocation points are always placed strictly inside the elements such that the surrounding surface is smooth. This has the advantage that the integral-free term $\mathcal{C}$ reduces to $\mathcal{C} = \frac{1}{2}\mathcal{I}$ which is significantly easier to compute than in the nodal collocation (see [24] for the expressions of $\mathcal{C}$ for three-dimensional elastostatics).

The final system of Eqs. (28) (or (36) for dynamic problems) is obtained by introducing the Neumann boundary conditions in a weighted sense by using the mass matrix B. Moreover, Robin boundary conditions are easily implemented by using another mass matrix G. This system is well structured in contrast to the nodal collocation approach where the system matrix is usually a mixture of columns of V and K. This mixture is often ill-conditioned and needs dimensionless variables to obtain reasonably small condition numbers. The condition numbers $\mathrm{cond}(\mathsf{A})$ given in subsection 6.1 are based on such variable transformations. Nevertheless, the condition numbers due to the proposed method are (with the exception of elastostatics) smaller than in the nodal collocation despite their larger sizes. This is especially the case in the dynamic analyses.

The Schur complement of systems (28) and (36) resembles a Dirichlet-to-Neumann map [38]. It has mapping properties similar to a finite element stiffness matrix and, therefore, is well-suited for the coupling of boundary with finite element methods. Such a coupling scheme, which is independent of the discretization method on the subdomain level, has been proposed in [33] based on the presented collocation method.

The new approach is based on the globally discontinuous approximation of q in Eq. (22) and treats every coefficient q_j of the approximation as an unknown quantity. For this reason the system matrices are significantly larger than in the nodal collocation. Consider for instance, the

case of three-dimensional elasticity with a piecewise linear discontinuous approximation of the tractions. In that case, every surface element τ_e has nine unknown traction coefficients and the dimension of the system matrix V is thus $(9N_e)^2$, where N_e denotes the number of elements. The presented formulation allows for the use of a piecewise constant traction approximation but, unfortunately, the combination of linear and constant shape functions spoils the solvability of the final system of equations [39]. Possibly, stabilization techniques known from mixed finite element methods [4] could be adapted to the system of this collocation approach such that the use of constant shape functions for the approximation of the dual variable q becomes feasible.

In any case, it can be assumed that matrix approximation techniques such as the adaptive cross approximation [3] (see also [32]) would yield good approximation rates if applied to the matrix V. Moreover, the use of iterative solution methods tailored to systems of the type (28) could significantly speed up the solution procedure because of the good condition numbers of the block matrices V and S. Such preconditioned iterative solvers are so far only available for the symmetric Galerkin method [40].

Another drawback of the proposed approach is the placement of the collocation points which is so far heuristic. It would be desirable to have a criterion at hand which is based on mathematical analysis.

8 Conclusion

A novel collocation approach has been presented with valuable properties. It combines the natural approximation spaces with a structured and well conditioned system matrix. Moreover, the inclusion of Robin boundary conditions is straightforward. But these features come with a high numerical cost such that the method in its current state can only be applied to rather small-sized problems. Nevertheless, this problem could be reduced. The use of iterative solvers with matrix compression techniques would significantly speed up the solution process and reduce the storage requirements.

References

[1] J.D. Achenbach. *Wave propagation in elastic solids*. North-Holland, 2005.

[2] E. Anderson, Z. Bai, C. Bischof, S. Blackford, J. Demmel, J. Dongarra, J. Du Croz, A. Greenbaum, S. Hammarling, A. McKenney, and D. Sorensen. *LAPACK Users' Guide*. Society for Industrial and Applied Mathematics, third edition, 1999.

[3] M. Bebendorf and S. Rjasanow. Adaptive low-rank approximation of collocation matrices. *Computing*, 70:1–24, 2003.

[4] M. Benzi, G.H. Golub, and J. Liesen. Numerical solution of saddle point problems. *Acta Numerica*, 14:1–137, 2005.

[5] D.E. Beskos. Boundary element methods in dynamics analysis. *Applied Mechanics Review*, 40:1–23, 1987.

[6] D.E. Beskos. Boundary element methods in dynamic analysis: Part II (1986-1996). *Applied Mechanics Review*, 50(3):149–197, 1997.

[7] R. Courant, K. Friedrichs, and H. Lewy. Über die partiellen Differenzengleichungen der mathematischen Physik. *Mathematische Annalen*, 100:32–74, 1928.

[8] M.G. Duffy. Quadrature over a pyramid or cube of integrands with a singularity at a vertex. *SIAM journal on Numerical Analysis*, 19:1260–1262, 1982.

[9] D.A. Dunavant. High degree efficient symmetrical Gaussian quadrature rules for the triangle. *International Journal for Numerical Methods in Engineering*, 21:1129–1148, 1985.

[10] L. Gaul, M. Kögl, and M. Wagner. *Boundary Element Methods for Engineers and Scientists*. Springer, 2003.

[11] G.H. Golub and C.F. van Loan. *Matrix Computations*. Johns Hopkins University Press, 1996.

[12] K.F. Graff. *Wave motions in elastic solids*. Dover Publications, 1991.

[13] F. Hartmann. *Introduction to Boundary Elements. Theory and Applications*. Springer, 1989.

[14] N.J. Higham. FORTRAN codes for estimating the one-norm of a real or complex matrix, with applications to condition estimation. *ACM Transactions on Mathematical Software*, 14:381–396, 1988.

[15] P.R. Johnston. Semi-sigmoidal transformations for evaluating weakly singular boundary element integrals. *International Journal for Numerical Methods in Engineering*, 47:1709–1730, 2000.

[16] L. Kielhorn and M. Schanz. CQM based symmetric Galerkin BEM: Regularization of strong and hypersingular kernels in 3-d elastodynamics. *International Journal for Numerical Methods in Engineering*, 2007. doi: http://dx.doi.org/10.1002/nme.2381.

[17] A.R. Krommer and C.W. Ueberhuber. *Computational Integration*. SIAM, 1998.

[18] V.D. Kupradze, T.G. Gegelia, M.O. Basheleishvili, and T.V. Burchuladze. *Three-dimensional Problems of the Mathematical Theory of Elasticity and Thermoelasticity*. North-Holland, 1979.

[19] J.C. Lachat and J.O. Watson. Effective numerical treatment of boundary integral equations: a formulation for three-dimensional elastostatics. *International Journal for Numerical Methods in Engineering*, 10:991–1005, 1976.

[20] J.D. Lambert. *Numerical Methods for Ordinary Differential Systems*. John Wiley & Sons, 1990.

[21] A.E.H. Love. *Treatise on the Mathematical Theory of Elasticity*. Dover Publications, 1944.

[22] C. Lubich. Convolution quadrature and discretized operational calculus I & II. *Numerische Mathematik*, 52:129–145 & 413–425, 1988.

[23] W.J. Mansur. *A time-stepping technique to solve wave propagation problems using the boundary element method*. PhD thesis, University of Southampton, 1983.

[24] V. Mantič. A new formula for the c-matrix in the Somigliana identity. *Journal of Elasticity*, 33:193–201, 1993.

[25] G. Of. *BETI-Gebietszerlegungsmethoden mit schnellen Randelementverfahren und Anwendungen*. PhD thesis, University of Stuttgart, 2006.

[26] F. París and J. Cañas. *Boundary Element Method*. Oxford University Press, 1997.

[27] C. Patterson and N.A.S. Elsebai. A regular boundary method using non-conforming elements for potentials in three dimensions. In C.A. Brebbia, editor, *Boundary Element Methods in Engineering*, pages 112–126, 1982.

[28] C. Patterson and M.A. Sheikh. Non-conforming boundary elements for stress analysis. In C.A. Brebbia, editor, *Boundary Element Methods*, pages 137–152, 1981.

[29] C. Patterson and M.A. Sheikh. Interelement continuity in the boundary element method. In C.A. Brebbia, editor, *Topics in Boundary Element Research*, pages 121–141. Springer, 1984.

[30] C.L. Pekeris. The seismic surface pulse. *Proceedings of the National American Society*, 41:469–480, 1955.

[31] W.H. Press, S.A. Teukolsky, W.T. Vetterling, and B.P. Flannery. *Numerical Recipes in C++*. Cambridge University Press, 2002.

[32] S. Rjasanow and O. Steinbach. *The Fast Solution of Boundary Integral Equations*. Springer, 2007.

[33] T. Rüberg. *Non-conforming FEM/BEM Coupling in Time Domain*, volume 3 of *Computation in Engineering and Science*. Verlag der Technischen Universität Graz, 2008.

[34] M. Schanz. *Wave propagation in Viscoelastic and Poroelastic Continua - A boundary element approach*. Springer, 2001.

[35] M. Schanz and H. Antes. A new visco- and elastodynamic time domain boundary element formulation. *Computational Mechanics*, 20:452–459, 1997.

[36] M. Schanz and L. Kielhorn. Dimensionless Variables in a Poroe lastodynamic Time Domain Bounday Element Formulation. *Building Research Journal*, 53(2–3):175–189, 2005.

[37] C. Schwab and W.L. Wendland. On numerical cubature of singular surface integrals in boundary element methods. *Numerische Mathematik*, 62:343–369, 1992.

[38] O. Steinbach. *Stability Estimates for Hybrid Domain Decomposition Methods*. Springer, 2003.

[39] O. Steinbach. Mixed approximations for boundary elements. *SIAM journal on Numerical Analysis*, 38:401–413, 2000.

[40] O. Steinbach. Fast solution techniques for the symmetric boundary element method in linear elasticity. *Computer Methods in Applied Mechanics and Engineering*, 157:185–191, 1998.

[41] O. Steinbach. *Numerical Approximation Methods for Elliptic Boundary Value Problems*. Springer, 2008.

[42] L.T. Wheeler and E. Sternberg. Some theorems in classical elastodynamics. *Archive for Rational Mechanics and Analysis*, 31:51–90, 1968.

[43] G. Yan and F.-B. Lin. Treatment of corner node problems and its singularity. *Engineering Analysis with Boundary Elements*, 13:75–81, 1994.